Slow water dynamics at the surface of macromolecular assemblies of different morphologies†

Pramod Kumar Verma, Ranajay Saha, Rajib Kumar Mitra* and Samir Kumar Pal*

Received 31st March 2010, Accepted 23rd July 2010
DOI: 10.1039/c0sm00188k

In this contribution we, for the first time, explore the slow dynamical states of confined water molecules in lamellar structures of AOT with various degrees of hydration using a picosecond resolved fluorescence spectroscopic technique using coumarin-500 as the fluorophore. A comparison of slow dynamics between AOT lamellar structures and AOT RMs have been made by preparing RMs that have a diameter the same as the interplanar water layer thickness of lamellar structures and the same number of water molecules in lamellar structures in order to understand the effect of morphology and hydration on the relaxation dynamics of water molecules in these nanoconfining systems. The relaxation time scales obtained in the lamellar systems differ to those of the RM systems and the difference of the timescales has been explained as a interplay between two opposing factors arising out of the morphology and interlayer distance, respectively. The geometrical restriction of the probe at the lamellar interface is determined by measuring time-resolved rotational anisotropy. The hydrogen bond energy of the water molecules residing at the lamellar interface is measured applying the Arrhenius type barrier crossing model.

Introduction

The structure and dynamics of water is very uniquely dependent on the environment it is associated with. In micro-heterogeneous systems, it exhibits various kinds of hydrogen bonding networks which provide a potential platform to understand the dynamic property of water in real biological systems. The hydrogen bonding network of water suffers significant modification when associated with an interface and the extent of modification is associated with the geometry of the interface. The nature of the binding and the exposure of water molecules to the surface play a key role in determining the dynamics of the system. Very commonly used and very well studied micro-heterogeneous systems are the self-aggregated amphiphilic macro-molecular assemblies like micelles, reverse micelles (RMs), vesicles, lamellae *etc.*, that potentially mimics many biological interfaces like proteins, DNA, cell membranes *etc.* The amphiphilic nature of the surfactant molecules drives them to curve against water in order to keep them away from the hydrophobic environment, and in order to do so produce different geometries like micelles, RM, lamellar liquid crystals, vesicles *etc.* The curved monolayer (or multilayer) of surfactant film around water brings about significant modification in the physiochemical nature of water molecules, and dynamics of such water molecules is markedly different compared to that of bulk water.

As has extensively been studied in micelles and RMs[1–6] the interfacial water tends to show remarkably slow dynamics compared to the bulk water. The very nature of hydrogen bonding at such an interface plays the most important role in the retarded dynamics. A vital question yet to be answered at this point of understanding is that how the curvature of the interfacial film affects the dynamics of water. As has previously been reported by many groups, it is only the confinement in the RM system that brings about the retarded relaxation of water.[6–9] Studies involving various techniques[2,8,10–22] infer the presence of different kinds of water molecules in RM depending upon the primary, secondary and tertiary hydrogen bonding with the interface. While bulk water relaxes within sub-picosecond time scale,[23] these water molecules take some hundreds of picoseconds to relax depending upon the extent of interaction with the interface.[3,6,7,24] As the amount of water starts increasing in the nanopool of RM, the curvature of surfactant film decreases and a smaller fraction of water interacts with the interface leading to relatively fast relaxation.[24–27] We have recently shown that if the film curvature can be modified by mixing of surfactants, dynamics of the confined water can be tuned.[28]

At this point it is very interesting to show how a flat interface does modify the dynamics of this confined water. A very well studied system consisting of flat surface is the lyotropic lamellar phase in which water layers of thickness ranging from 1.5 to 19 nm are separated by flat surfactant bilayer.[29] Phase behaviour and physiochemical properties of water confined in AOT lamellar system has previously been examined using various techniques.[29–33] Pulse field gradient spin echo-NMR study (PFGNMR)[34] shows that the self diffusion co-efficient of water in AOT lamellar system varies from 7.7 to 8.6 $\times$ 10^{-10} m^2 s^{-1}, which is an order of magnitude higher than that of bulk water but smaller than that observed in RM systems.[35–37] This makes the dynamics of water in lamellar systems a very interesting phenomenon to be investigated and compared with other self-aggregating systems, which is unfortunately lacking in the

Unit for Nano Science & Technology, Department of Chemical, Biological & Macromolecular Sciences, S.N. Bose National Center for Basic Sciences, Block JD, Sector III, Salt Lake, Kolkata, 700098, INDIA. E-mail: skpal@bose.res.in; rajib@bose.res.in

† Electronic supplementary information (ESI) available: Details of the solvation dynamics and difference absorption spectra. See DOI: 10.1039/c0sm00188k

present literature. Very recently Fayer *et al.*[38] compared the water dynamics in AOT lamellar structure and RM using Infrared (IR) pump probe technique in order to understand the effects of geometry and nanoscale layer separation on the dynamics. They studied four lamellar systems and compared the results with eight RM systems, four with identical interlayer distances as those of the lamellae (*i.e.*, $d = l$, where, d is the diameter of the RM nanopool and l is the interlayer distance in the lamellae) and the other four with the identical hydration ($w_0 = L_0$ where w_0 and L_0 are the water to surfactant molar ratio in RM and lamellae, respectively *i.e.*, w_0 = [water]/[AOT] in reverse micellar systems and L_0 = [water]/[AOT] in lamellar systems). They measured the IR stretching relaxation of water molecules around the AOT surface and the comparisons with the RM systems were made only based on the ultrafast population relaxation (timescale of ~4 ps) and orientational relaxation (~20 ps) dynamics of water. The vibrational population relaxation and orientational relaxation timescales are equivalent for lamellar and RM system with the same degree of hydration ($w_0 = L_0$). However, the fraction of interfacial molecules associated with the population relaxation is always higher for the lamellar systems with respect to the RM system. This is also true for the fraction of water molecules undergoing wobbling motion at the interface. They concluded that the primary factor that governs the properties and dynamics of water in such systems is the water to surfactant interaction, which in turn is a manifestation of the geometry of the surface.

In view of the results on the fast vibrational relaxation in these systems as reported by Fayer *et al.*,[38] it would be interesting to understand the diffusion controlled slow relaxation process in these systems and the effect of surface geometry on them. In order to complement the results on the fast dynamics of water in lamellar systems obtained by Fayer *et al.*,[38] we, in this present report, investigate the slow dynamics of water in AOT lamellar structure using picosecond-resolved fluorescence spectroscopic technique and compared the results with those obtained for the RM systems. To the best of our understanding this is the first report on the slow water relaxation dynamics of AOT lamellar systems. Following the phase behaviour of AOT/water binary system,[39] we select four compositions with 35%, 40%, 50%, and 60% of AOT (w/w) which corresponds to $L_0 = 46$, 37, 25 and 16.5 respectively. The choice of these compositions lies on the fact that the interlayer distance in these compositions are known from X-ray diffraction studies[29,30] which are 4.0, 3.3, 2.3 and 1.6 nm respectively and the ultrafast water relaxation in these systems has previously been reported by Fayer *et al.*[38] To understand the effect of curvature (geometry) and the extent of hydration on the dynamics of such systems, we compare the results obtained from the lamellar systems with those from RM systems with the same hydration level ($L_0 = w_0$) with w_0 values of 46, 37, 25 and 16.5 respectively, and same interlayer distances with w_0 values of 10, 7.6, 5 and 2 respectively. The fluorophore used in the present investigation is Coumarin 500 (Scheme 1), which has a unique feature that if excited at 409 nm, the fluoroprobes residing at the AOT-water interface get selectively excited, and thus the fluorescence information comes solely from the interface. Linear dichroism (LD, the differential absorbance of light polarized parallel and perpendicular to an orientation direction) spectra have also been obtained to probe the orientation of C-500 in lamellar bilayers. To understand the geometrical restriction of the probe at the interface, rotational relaxation dynamics of the dye in different RM systems have also been determined. We have also investigated the dynamics of water in AOT lamellar structures as a function of temperature and calculated the energy barrier of the bound to free water transition following an Arrhenius type barrier crossing model.[40–42]

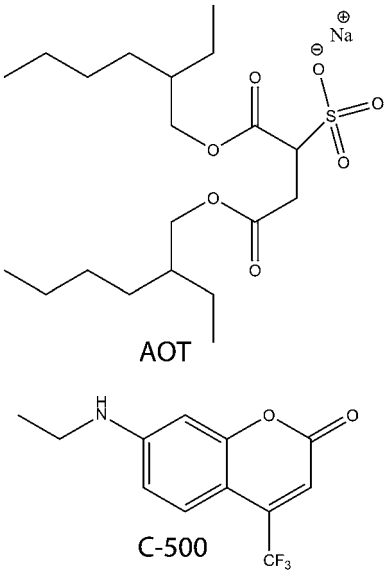

Scheme 1 Molecular structure of AOT (Sodium bis(2-ethylhexyl)sulfosuccinate) and coumarin 500 (C-500)

Materials and methods

Sodium bis(2-ethylhexyl)sulfosuccinate (AOT) and isooctane (i–Oc) were purchased from Sigma and used as received. Coumarin 500 (C-500) (Scheme 1), was a product of Exciton. AOT lamellar structures were prepared by mixing a calculated weight of AOT with required volumes of water containing the fluorophore, sealed in a container, heated to 50 °C and centrifuged back and forth to ensure complete mixing. Required states of hydration are expresed as $L_0 = [H_2O]/[AOT]$, the number of water molecules per surfactant molecule in lamellar structures. All the samples were equilibrated at 20 ± 1 °C for at least 20 days before carrying out any measurements. The reverse micelle (RM) solutions of C-500 were prepared by adding calculated volumes of water into a given volume of 500 mM AOT solution in isooctane containing the fluorophore with vigorous stirring to achieve RMs with required degree of hydration, $w_0 = [H_2O]/[AOT]$.

Steady–state absorption and emission were measured with a Shimadzu UV-2450 spectrophotometer and a Jobin Yvon Fluoromax-3 fluorimeter, respectively with a temperature controlled attachment from Julabo (Model: F32). Fluorescence transients were measured and fitted by using commercially available spectrophotometer (LifeSpec-ps) from Edinburgh Instrument, U.K. (excitation wavelength 409 nm, 80 ps instrument response function (IRF)) with a temperature controlled attachment from Julabo (Model: F32). The observed fluorescence transients are fitted by using a nonlinear least square fitting

procedure to a function $(X(t) = \int_0^t E(t')R(t-t')dt')$ comprising of convolution of the IRF (E(t)) with a sum of exponentials $\left(R(t) = A + \sum_{i=1}^{N} B_i e^{-t/\tau_i}\right)$ with pre-exponential factors (B_i), characteristic lifetimes (τ_i; the lifetime τ is the time needed for the concentration of molecular entities to decrease to 1/e of its original value as per the eqn $I = I_0 \exp(-t/\tau)$) and a background (A). Relative concentration in a multi-exponential decay is finally expressed as; $a_n = B_n / \sum_{i=1}^{N} B_i$. The quality of the curve fitting is evaluated by reduced chi-square (χ^2) and residual data.

To construct time-resolved emission spectra (TRES) we follow the technique described in ref. 43 and 44. As described above the emission intensity decays are analyzed in terms of the multi-exponential model,

$$I(\lambda, t) = \sum_{i=1}^{N} \alpha_i(\lambda)\exp[-t/\tau_i(\lambda)] \quad (1)$$

where $\alpha_i(\lambda)$ are the pre-exponential factors, with $\Sigma\alpha_i(\lambda) = 1.0$. In this analysis, we compute a new set of intensity decays, which are normalized so that the time-integrated intensity at each wavelength is equal to the steady-state intensity at that wavelength. Considering $F(\lambda)$ to be the steady-state emission spectrum, we calculate a set of $H(\lambda)$ values using,

$$H(\lambda) = \frac{F(\lambda)}{\int_0^\infty I(\lambda, t)dt} \quad (2)$$

which for multi-exponential analysis becomes,

$$H(\lambda) = \frac{F(\lambda)}{\sum_i \alpha_i(\lambda)\tau_i(\lambda)} \quad (3)$$

Then, the appropriately normalized intensity decay functions are given by,

$$I'(\lambda, t) = H(\lambda)I(\lambda, t) = \sum_{i=1}^{N} \alpha'(\lambda)\exp\left(\frac{-t}{\tau_i(\lambda)}\right) \quad (4)$$

where $\alpha'_i(\lambda) = H(\lambda)\alpha_i(\lambda)$. The values of $I'(\lambda,t)$ are used to calculate the intensity at any wavelength and time, and thus the TRES. The values of the emission maxima and spectral width are determined by nonlinear least-square fitting of the spectral shape of the TRES. The spectral shape is assumed to follow a lognormal line shape,[44]

$$I(\bar{\nu}) = I_0 \exp\left\{-\left[\ln 2\left(\frac{\ln(\alpha+1)}{b}\right)^2\right]\right\} \quad (5)$$

with $\alpha = \frac{2b(\bar{\nu} - \bar{\nu_{max}})}{b} > -1$, where I_0 is amplitude, $\bar{\nu}_{max}$ is the wavenumber of the emission maximum and spectral width is given by, $\Gamma = \Delta[sinh(b)/b]$

The terms b and Δ are asymmetry and width parameters. The eqn (5) reduces to a Gaussian function for $b = 0$.

The time dependent fluorescence Stokes shifts, as estimated from TRES (Time Resolved Emission Spectroscopy), were used to construct the normalized spectral shift correlation function or the solvent correlation function C(t) defined as

$$C(t) = \frac{\nu(t) - \nu(\infty)}{\nu(0) - \nu(\infty)} \quad (6)$$

where $\nu(0)$, $\nu(t)$ and $\nu(\infty)$ are the emission maxima (in cm^{-1}) at time zero, t and infinity, respectively. The C(t) function represents the temporal response of the solvent relaxation process, as occurs around the probe following its photo excitation and the associated change in the dipole moment. C(t) when plotted against time, can be fitted with mono- or multi-exponential decay parameters providing the time constants (τ_i) and their relative weightage (a_i). For anisotropy ($r(t)$) measurements, emission polarization is adjusted to be parallel or perpendicular to that of the excitation, and anisotropy is defined as

$$r(t) = \frac{I_{II}(t) - GI_{\perp}(t)}{I_{II}(t) + 2GI_{\perp}(t)} \quad (7)$$

G, the grating factor, was determined following long time tail matching technique.[45] All the anisotropies were measured at the emission maxima.

Arrhenius type of activation energy barrier crossing model has been used to calculate the activation energy barrier (E_{act}) for bound water-to-free water interconversion using the following relation,[40,46]

$$\frac{1}{<\tau>} \approx k_{bf} = A\exp\left(-\frac{E_{act}}{RT}\right) \quad (8)$$

here, $<\tau>$ represents the average solvation time constant ($<\tau> = \sum_i a_i\tau_i$), k_{bf} is the rate of bound-to-free water conversion, A is the pre-exponential factor and E_{act} is the corresponding activation energy for the transition process. A plot of $\ln(1/<\tau>)$ against $1/T$ produces a straight line and from the slope of the line E_{act} can be calculated.

Results and discussion

Fig. 1 depicts the absorption and linear dichroism (LD) spectra of the probe C-500 in the four lamellar structures and eight RMs. Each panel of the Fig. 1 groups the spectrum of a lamellar structure (solid lines) with two RMs spectra (broken lines) one of which has the same extent of hydration as the lamellar structure (*i.e.*, $w_0 = L_0$) and the other one has the diameter equal to the interlayer distance of the lamellar structure. In contrast to ordinary absorption dichroism, LD, detects oriented chromophores only. As evident from Fig. 1, there is a positive LD signal of the visible wavelength transition of C-500 in lamellar structures which is absent in all the RM systems. Note that the probe C-500 binds to the interface of lamellar or RM. However, the LD signal coming from the probe within the RM (Fig. 1) is zero revealing the dynamical nature of the RMs. Thus, the LD study confirms the formation of lamellar structures. The absorption curves of the systems are rather featureless producing a peak at ~400 nm for all the lamellar systems.

The fluorophore C-500 is sparingly soluble in water and shows reasonably good solubility in isooctane. Earlier reports[47,48] from our group have shown that in bulk water the absorption peak of C-500 (400 nm) is significantly red-shifted (shifted toward higher

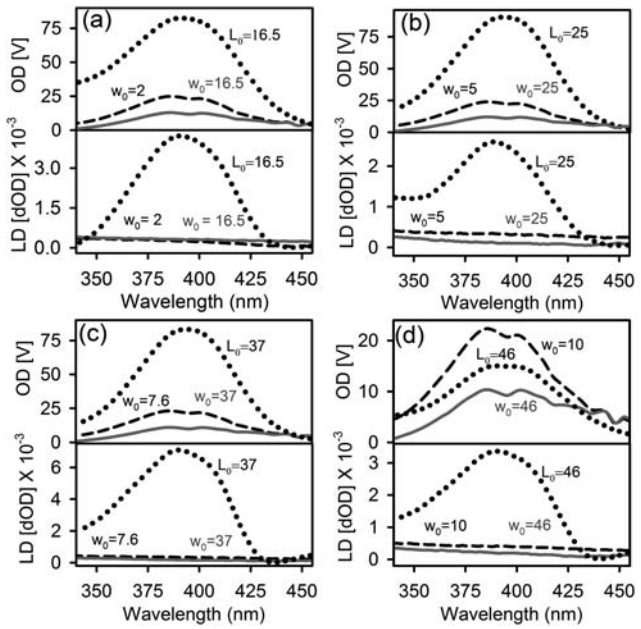

Fig. 1 Absorbance and linear dichroism (LD) spectra of AOT lamellar structures and RMs. Each panel groups the spectrum of a lamellar structure (solid lines) with two RMs spectra (broken lines), one with the same diameter as the surface-to-surface distance of the lamellar structure ($w_0 \neq L_0$) and other that has the same number of water molecules per AOT, $w_0 = L_0$. The positive LD signals being present in the case of lamellar signifies the presence of oriented C-500 in lamellae. LD signals are absent for the RMs as they are dynamic in nature (continuous process of breaking and reformation).

wavelength) compared to that in isooctane (360 nm). The emission peak of C500 in bulk water (500 nm) also shows a 90 nm red shift compared to that in isooctane (excitation at 350 nm). The significantly large solvatochromic effect (solvation) in the absorption and emission spectra of C-500 in polar and nonpolar

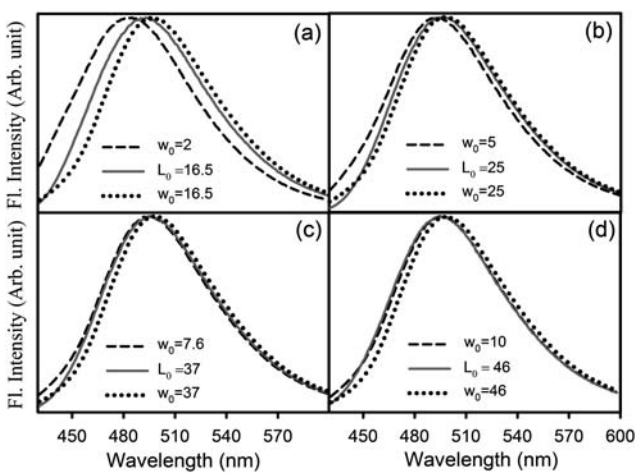

Fig. 2 Normalized emission spectra of C-500 in AOT lamellar structures and RMs. Each panel groups the spectrum of a lamellar structure (solid curves) with two RMs spectra (broken curves). The two RMs spectra are the spectrum of the RM that has the same diameter as the surface-to-surface distance of the lamellar structure ($w_0 \neq L_0$) and the spectrum of the RM that has the same number of water molecules per AOT, $w_0 = L_0$.

Table 1 Steady-state fluorescence peak (λ_{max}), fittings parameters of the solvent correlation function ($C(t)$) for probe C-500 in lamellar structures and RMs of various L_0 and w_0 values at different temperatures. τ_i's are the time components and a_i's are the weightage factors. $<\tau>$ is given as, $<\tau> = \sum_i a_i \tau_i$

Size	T/K	Fluorescence peak (λ_{max})/nm	a_1	τ_1/ns	a_2	τ_2/ns	$<\tau>$/ns
$L_0 = 16.5$	293	492	0.35	0.31	0.65	1.40	1.01
$w_0 = 2$	293	484	0.27	0.34	0.72	3.65	2.73
$w_0 = 16.5$	293	497	0.62	0.31	0.38	1.27	0.67
$L_0 = 25$	293	495	0.48	0.48	0.52	1.51	1.02
$w_0 = 5$	293	492	0.37	0.19	0.63	1.80	1.20
$w_0 = 25$	293	498	0.42	0.12	0.58	0.81	0.52
$L_0 = 37$	278	493	0.40	0.40	0.60	2.21	1.49
	293	495	0.58	0.42	0.42	1.59	0.92
	308	497	0.73	0.30	0.27	1.66	0.68
	323	497	0.74	0.19	0.26	1.47	0.53
	343	497	0.78	0.16	0.22	1.40	0.44
$w_0 = 7.6$	293	495	0.44	0.28	0.56	1.44	0.93
$w_0 = 37$	293	499	0.34	0.08	0.66	0.63	0.45
$L_0 = 46$	278	495	0.32	0.34	0.68	1.95	1.43
	293	497	0.59	0.34	0.41	1.43	0.78
	308	497	0.66	0.16	0.34	0.85	0.40
	323	497	0.79	0.25	0.21	0.81	0.36
	343	497	0.41	0.11	0.59	0.32	0.23
$w_0 = 10$	293	495	0.55	0.34	0.45	1.45	0.83
$w_0 = 46$	293	499	0.62	0.23	0.38	0.89	0.48

medium makes the dye an attractive probe for microenvironments. To justify the excitation wavelength of 409 nm, we construct difference absorption spectra of C-500 in AOT RMs and lamellar (with respect to C-500 in i–Oc) (Figure S1 in the supporting information section†). As can be observed from the figure, a single peak is obtained at 400 nm, which is the signature of the C-500 molecules in the vicinity of the AOT–water interface to be excited. Fig. 2 is a representative illustration of the emission spectra of C-500 in various L_0 and w_0 values at 298 K excited at 409 nm. The corresponding emission peaks (λ_{max}) of the fluorescence spectra are presented in Table 1. As evidenced from Table 1, $L_0 = 16.5$ produces an emission peak at 492 nm which suffers progressive red shift with increasing water content (L_0) with an observed λ_{max} of 497 nm at $L_0 = 46$. It is important here to note that the λ_{max} values are blue shifted compared to that observed in bulk water (~515 nm) indicating that the water molecules reside in a highly restricted environment, as has previously been observed in RMs.[49] Similar reports were observed from the static spectroscopic studies of Wong *et al.*,[50,51] where the polarity of the water pool increases as the RM size increases. They attributed this increased polarity to an increase in the number of bulk-type water molecules in the water pool.

It is interesting to note that at low hydration level of the lamellar systems ($L_0 = 16.5$ and 25), the λ_{max} values obtained are red shifted compared to those obtained in the RM systems with comparable interlayer distance ($w_0 = 2$ and 5), and blue shifted compared to those of RM systems with comparable hydration ($w_0 = 16.5$ and 25). However, at higher hydration ($L_0 = 37$ and 46), the λ_{max} values are comparable with those of the RM systems. The gradual increase in the λ_{max} values with increasing L_0 signifies a more polar environment experienced by the fluorophore. It has previously been observed for AOT RM systems that C-500 shows a red shift with increasing hydration to reach

a constant value of ~499 nm.[49] In the present study, for larger RM systems ($w_0 \geq 16.5$), the λ_{max} values obtained are in the range of 497–499 nm. For much larger RM systems, a definite water pool has already been formed and with further increase in w_0, the probe hardly experiences any change in the polarity. Thus the λ_{max} values also suffer insignificant change. On the other hand, at low hydration level ($w_0 = 2$ and $L_0 = 16.5$), the interlayer distance is 1.6 nm, which can accommodate only 5-6 layers of water molecules compared to 20–70 layers of water molecules at higher hydration level ($w_0 = 16.5$ to 46). Thus for $L_0 = 16.5$ and $w_0 = 2$, the water molecules are strongly interacting with the AOT surface, resulting in a lower polarity and consequently blue shifted λ_{max} values. Comparison between the RM and lamellae at low hydration shows that $(\lambda_{max})_{RM}$ is blue shifted compared to the $(\lambda_{max})_{Lamellar}$ values. Earlier DSC (differential scanning calorimetry) studies showed that the number of unfreezable water molecules is equal in AOT lamellae and RM[31,52] and there are same numbers of water molecules per AOT molecule in both the systems. The major difference between the two systems is the effective surface area of AOT.[30,53] The curved nature of the interfacial film of AOT in RM system compared to the flat surface in lamellae provides more exposure of the carbonyl ester group of AOT towards water making the hydrogen bonding stronger in RM. This phenomenon is strongly reflected in the lower λ_{max} values of RM compared to lamellae with the same intersurface distance and faster water relaxation (see later). It could be noted here that the results obtained from the O–D stretching frequency spectra of identical systems as observed by Fayer *et al.*[38] are considerably different than our steady state fluorescence results. As per their results the O–D stretching frequency spectra of lamellar systems overlap with those of RM systems having the same degree of hydration (*i.e.*, $L_0 = w_0$) while that of RM with equal interlayer distance ($d = l$, $w_0 < L_0$) shows a peak at higher frequency. This ambiguity can easily be understood in light of the origin of IR and fluorescence spectrum. While the IR frequency is strongly dependent on the O–D stretching and bending modes and thus on much localized hydrogen bonding network of the interfacial water molecules, fluorescence spectrum provides information on the average environment experienced by the fluorophore upon excitation. In the present study, the fluorophore used is C-500 and as has been discussed earlier, excitation at 409 nm excites molecules residing at the interface only. Thus the fluorescence spectrum as obtained in the present study reflects the collective nature of the local microenvironment around the AOT interface and thus the difference in the peak position at different L_0 and w_0 values. At higher hydration, the probe can hardly differentiate between the interfacial and bulk type water molecules and thus comparable λ_{max} values are obtained for all the systems (Table 1).

The probe C-500 has previously been used to report the solvation dynamics of AOT/i-Oc RM system at various degrees of hydration at different temperatures.[49,54] Here, we study the solvation dynamics of the probe in AOT lamellar systems at different L_0 and temperature and compared the result with those obtained from the RMs with equivalent hydration and interlayer distance. Fluorescence decay transients of C-500 in $L_0 = 37$ system at 293 K at three selected wavelengths of 430 (at the blue end of the spectrum), 490 (at the peak position), and 600 (at the red end of the spectrum) nm are shown in the inset of Fig. 3c. It is evidenced from the Figure that the decay pattern is strongly

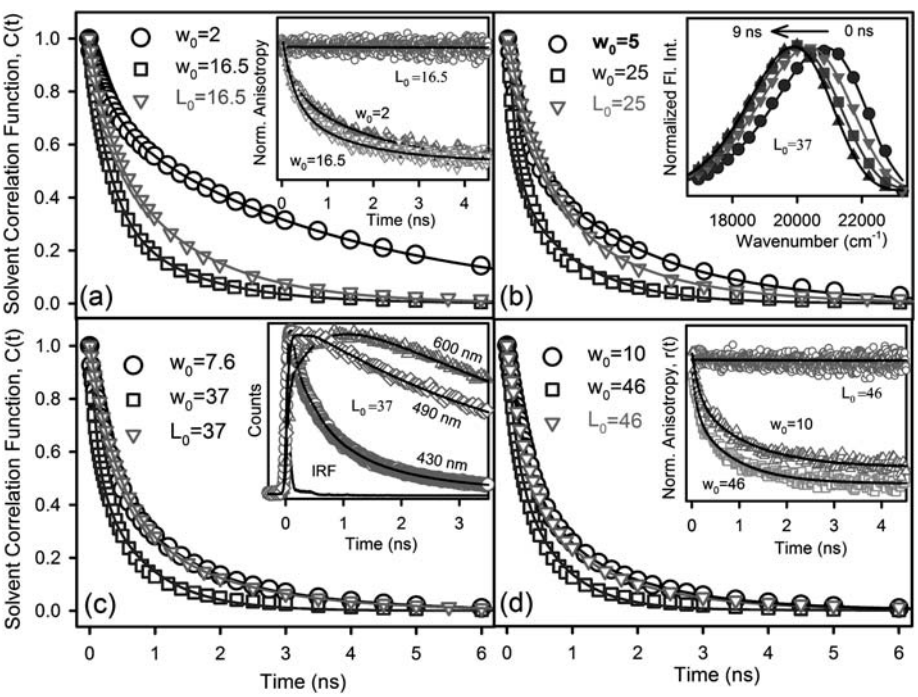

Fig. 3 Solvation correlation function, $C(t)$, in AOT lamellar structures and RMs. Each panel groups the spectrum of a lamellar structure (△) with two RMs spectra (○ and □), one with the same diameter as the surface-to-surface distance of the lamellar structure ($w_0 \neq L_0$) and the other with the same number of water molecules per AOT, $w_0 = L_0$. Inset of Figure 3c represents the fluorescence decay transients of C-500 in lamellar structure with $L_0 = 37$ at 293 K and its corresponding time-resolved emission spectra (TRES) is shown in the inset of Figure 3b. The inset of Figure 3a and 3d shows the time resolved anisotropy decay, $r(t)$, of C-500 at lower hydration, $L_0 = 16.5$ (with $w_0 = 2$ and 16.5) and higher hydration, $L_0 = 46$ (with $w_0 = 10$ and 46).

wavelength dependent. At 293 K, the blue end (430 nm) decays with the fitted four-exponential time constants of 0.05 ns (39%), 0.31 ns (39%), 1.09 ns (27%) and 4.6 ns (5%). The transients get slower with increasing wavelength. For the extreme red wavelength (600 nm), a distinct rise component of 0.8 ns is produced along with a decay component of 4.9 ns. With increase in hydration (L_0), the transients at a particular wavelength and temperature become faster. This observation is attributed to the increased solvent mobility as the interlamellar water layer thickness expands, leaving proportionately lesser fraction of water bound to the lamellar interface.

Using the decay transients at different wavelengths, we construct the time resolved emission spectra (TRES) (as discussed earlier) for different L_0 and w_0 values at different temperatures. A representative TRES for C-500 at 298 K with $L_0 = 37$ is presented in the inset of Fig. 3b wherein a significant dynamic fluorescence Stokes shift of 962 cm^{-1} in 9 ns is observed. The solvent correlation function, $C(t)$ as obtained from eqn (6) for all these systems are presented in Fig. 3 (a–d). Each panel of Fig. 3 groups the $C(t)$ curves of lamellar structures ($d = l$; △) with two RM systems: one with the same diameter as the surface-to-surface distance of the lamellar structure (○) the other with the same number of water molecules per AOT, ($w_0 = L_0$; □). All the C(t) curves are well fitted with bi-exponential decay functions based on the core-shell model and the fitted parameters are presented in Table 1. The core-shell model is based on the fact that at least two distinctly different kinds of water molecules are present inside the RMs and lamellar, that is, interfacial (shell) water molecules directly hydrogen bonded to the headgroups, which displays modified properties compared with bulk water and very slow relaxation dynamics (in the order of nanoseconds), and interior (core) or bulk-like water, which are not directly hydrogen bonded to the surfactant headgroups but have properties slightly different from bulk water.[9,55–58] Note that both these two types of water molecules relax at a time scale slower than that of bulk water (of the order of sub picoseconds[23]), which is probably due to the confinement effect. It is evident from Table 1 that for all the lamellar structures at room temperature one of the solvation time constants is of the order of several hundreds of picoseconds, while the other is of the order of a few nanoseconds. At low water content ($L_0 = 16.5$ at 298 K) the decay consists of a slow time constant of 1.40 ns (65%) and a fast time constant of 0.35 ns (35%) with an average life time, $<\tau> = 1.01$ ns, where $<\tau> = a_1\tau_1 + a_2\tau_2$. On the other hand, at higher hydration ($L_0 = 46$ at 298 K) the $C(t)$ is still bi-exponential but decays faster with time components of 1.43 ns (41%) and 0.34 ns (59%) providing $<\tau> = 0.78$ ns. It could be noted here that both the observed time constants are orders of magnitude slower than the sub-picosecond solvation time constant of bulk water.[23] The observed slow and fast components generate out of the relaxation process by the interfacial bound type and free type water molecules, respectively present in the lamellar structure. A similar two-component model consisting of a shell of interfacial water molecules and a bulk-like core has previously been applied to explore the slow dynamics of the water molecules inside the RM.[3,6,9,42,49,59] However, such studies with lamellar structure have never been reported before.

Let us now compare the slow relaxation dynamics of water obtained in the different morphologies, which has been summarised in Table 1 and Fig. 4. As can be observed from Fig. 4, the general trend that follows in the dynamics of these systems is that, RMs with large hydration ($w_0 \geq 16.5$) have faster dynamics in all the studied systems, and do not change appreciably upon increasing hydration, *e.g.* $<\tau>$ value decreases from 0.67 ns for $w_0 = 16.5$ to 0.48 ns for $w_0 = 46$, while the interlayer distance (diameter of the RM) suffers ~4 fold increase. On the other hand, the RM systems with least hydration ($w_0 = 2$ and 5) show very slow relaxation ($<\tau> = 2.73$ and 1.2 ns respectively). The relaxation time constant of water molecules in lamellar systems lies in between these two systems. With moderate hydration ($L_0 = 37$ and 46), the $<\tau>$ values are identical to those of $w_0 = 7.6$ and 10, (RMs with equal interlayer distances of 3.3 and 4.0 nm respectively), but considerably slower than the RM systems with $w_0 = L_0$ (Table 1, Fig. 4). At high AOT concentration ($L_0 = 16.5$ and 25), the $<\tau>$ values are slower than those of $w_0 = 2$ and 5 (with interlayer distances of 1.6 and 2.3 nm respectively). To interpret this result we must first understand the origin of this slow relaxation process. IR studies by Boissière *et al.*[29] in AOT lamellar systems proposed the presence of three types of water, namely interfacial bound type water (IBW, water molecules bound to two other molecules), interfacial free type water (IFW, water molecules that bind with three neighbouring counterparts) and bulk type water (BW) (Scheme 2). While the contribution of IBW does not evolve as a function of L_0, the contribution of IFW decreases while that of BW increases until $L_0 = 46$ and then reaches a plateau. DSC and NMR study also confirmed the presence of three types of water in lamellar structures.[31] DSC[31] studies indicate that there is no bulk like water present at the $L_0 = 16.5$ and the fraction of BW gradually increases with increase in L_0. A similar distribution of water molecules has also been reported for the RM systems wherein sub-picosecond to a few ps relaxation of water molecules could only be obtained in the bulk like water molecules, which is present only if a well-defined water-pool inside RM is formed.[27,49] On the other hand, owing to the heterogeneous bonding with the surfactant interface, IFW and IBW make the relaxation process slow. As hydration (w_0 or L_0) increases, the

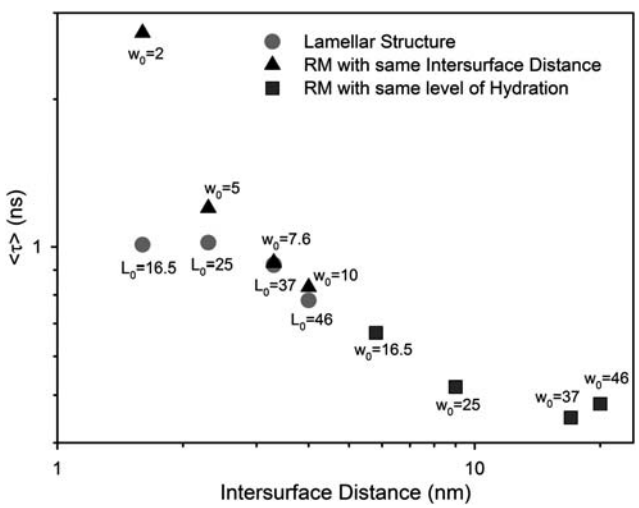

Fig. 4 Average time constants $<\tau>$ *versus* inter-surface distance of four lamellae and eight RMs (shown in log scale).

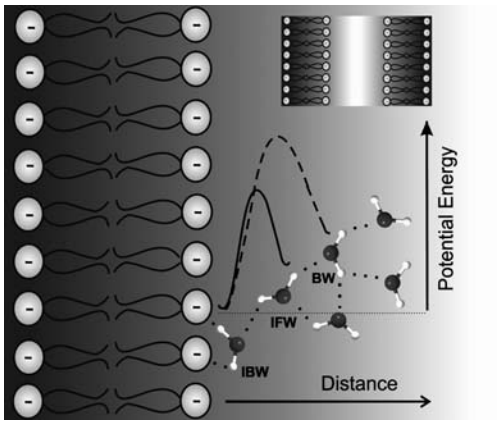

Scheme 2 Pictorial representation of the three different types of water namely interfacial bound water (IBW, water molecules hydrogen bonded to AOT headgroups), interfacial free water (IFW, water molecules hydrogen bonded to IBW) and bulk type water (BW), respectively. Note that activation energy (E_{act}) is smaller for IBW to IFW transition compared to the BW transition.

fraction of IFW and IBW decreases, at the expense of bulk water, and dynamics gets faster. Let us now compare the results of lamellar and RM systems with the same degree of hydration ($w_0 = L_0$). In all the cases, $<\tau>$ is almost two fold slower in the lamellar systems compared to the RM systems (Table 1, Fig. 4). It should be taken into consideration that the interlayer distance in the RM systems are 4-5 folds higher than the lamellar systems. Thus the fraction of bulk type water is considerably higher in the RM systems compared to the corresponding lamellar systems. It could be mentioned here that the diffusion coefficient of water in the RM system is lower compared to that of lamellar systems and also the hydrogen bond strength is higher in the former compared to the latter.[34,38] These factors tend to make the relaxation process faster in the lamellar system. Thus the total dynamics of the process is an optimization of the two opposing process and at this higher hydration level, the factor of interlayer distance prevails over the diffusion and hydrogen bond strength factors resulting in overall slow dynamics in the lamellar systems. Now let us consider the systems with the same interlayer distance ($d = l$) but different hydration ($L_0 > w_0$). As evidenced from Table 1 and Fig. 4, the $<\tau>$ values are very slow for $w_0 = 2$ and 5 systems compared to the $L_0 = 16.5$ and 25 systems. As the interlayer separation in these two systems are comparable (1.6 and 2.3 nm respectively), around 5–8 layers of water molecules can be accommodated between the two layers, which are just enough to hydrate the AOT head groups. So, at this hydration level, no bulk type water is formed and relaxation is mainly due to the IFW and IBW molecules. At this point the diffusion of the restricted water and also the strength of hydrogen bond play a key role in determining the relaxation dynamics, and eventually due to the curved nature of the interface followed by stronger hydrogen bonding, the solvation is considerably retarded in the RM system compared to the lamellar systems. At moderate hydration level ($w_0 = 7.6$ and 10) where the interlayer distances are 3.3 and 4.0 nm respectively, and 12–14 water molecules could be accommodated between the two layers, the first trace of fast moving bulk water appears making the dynamics faster. In these systems, the interplay between the presence of bulk water and the retarding factors perhaps nullifies each other resulting in a comparable $<\tau>$ values for both lamellar and RM systems. It could be noted here that the results obtained from Fayer *et al.*[38] shows a trend equivalent to our present study for the low hydration region ($L_0 = 16.5$ and 25), but differs in the moderate hydration region where lamellar systems ($L_0 = 37$ and 46) show considerably slower population relaxation than the corresponding RM systems ($w_0 = 7.6$ and 10). It should be taken into consideration that the vibration relaxation as measured by Fayer *et al.*[38] is bond specific (at 2548 cm^{-1}) and can provide very localized information, whereas the fluorophore experiences interactions by different types of water molecules and brings about average information of the total system. Thus the slow relaxation process in the present study complements the ultrafast vibrational relaxation dynamics reported by Fayer *et al.*[38] for identical systems.

To ascertain the geometrical restriction of the probe in the interfacial region, we measure the time-resolved anisotropy of the probe in both lamellar structures and AOT RMs of comparable surface to surface distance and water to surfactant ratio. Typical anisotropy decays are shown in the inset of Fig. 3a and 3d. The anisotropy decay transients have been fitted bi-exponentially for the RMs. The rotational time constants observed (data not shown) are of the order of hundreds of picoseconds and a few nanoseconds, which are in the same order of magnitude as previously reported for AOT RM systems.[49] However in the case of lamellar structures, the anisotropy does not decay within the experimental time window of 20 ns at lower hydration (inset of Fig. 3a, $L_0 = 16.5$) as well as higher hydration (inset of Fig. 3d, $L_0 = 46$). This indicates the rigid and orientated nature of the probe in the lamellar structure and is consistent with the LD data (Fig. 1). As has been reported by Fayer *et al.*[38] the wobbling motion of the probe in the lamellar structure is ultrafast (in the order of 20 ps), which is beyond the resolution of our instrumental resolution. However, with increases in temperature, a fast rotational relaxation component (of the order of a few hundreds of ps) is produced (not exemplified), which might be due to the transition of the probe from the rigid lamellar interface to bulk type water. The rotational relaxation for $L_0 = 37$ system at high temperature (60 °C) can be fitted bi-exponentially with time components of 0.12 and 0.62 ps, which is very much comparable to the fitted data for the $w_0 = 37$ system at room temperature (0.15 and 0.72 ns). It is interesting to note here that the $<\tau>$ values are also identical in these two cases (0.44 and 0.45 ns respectively, Table 1). Thus with increase in temperature, the geometrical restriction of the probe in the lamellar surface is released and becomes comparable to that of the RM systems with equivalent hydration.

To compare the hydrogen bond energy of water molecules at the AOT interface in lamellar structure with those in the RM systems, we measure the solvation dynamics with $L_0 = 37$ and 46 at different temperatures and the corresponding $C(t)$ curves at different temperatures are shown in Fig. 5. As the temperature is increased to 343 K, the transients still show wavelength dependency, however, the time constants get faster. Such faster decay transients with increasing temperature indicate the increased mobility of the solvating species at elevated temperatures, a trend similar to that observed in RMs.[42,49] We construct the TRES and

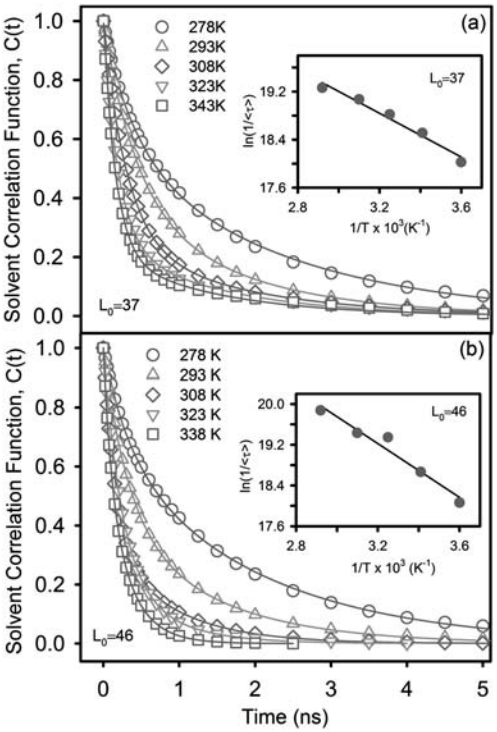

Fig. 5 Solvation correlation function, $C(t)$, of C-500 in AOT lamellar structure with interlayer distance of 3.3 nm (L_0 = 37) and 4.0 nm (L_0 = 46) at different temperatures. Note that with increasing temperature, the dynamics become faster. The solid lines are exponential fits. Insets show plot of ln(1/<τ>) against 1/T for AOT lamellar structures with L_0 = 37 and 46, with linear fits (solid lines).

the $C(t)$ fitting data are presented in Table 1. It can be observed that <τ> becomes faster with increasing temperature. This accelerated dynamics can be explained with the help of the multishell continuum model proposed by Bagchi *et al.*[40,60–63] for RMs and biomolecules in which an equilibrium of a dynamic exchange between free and bound water molecules is considered. The energetics of the exchange depends upon the strength and the number of hydrogen bonds among the water molecules at the interface. The bound to free type transition of water molecules with temperature follows an Arrhenius type of activation energy barrier crossing model[40–42] which has previously been exemplified by our group for different micro-heterogeneous systems.[42,49,64] We fit an Arrhenius plot using the <τ> values listed in Table 1 for L_0 = 37 and L_0 = 46, respectively, which produces good linear fits (Fig. 5) with corresponding activation energy values of 3.6 and 5.2 kcal mol^{-1} for L_0 = 37 and 46 systems, respectively. We previously obtained the E_{act} value of 3.4 and 4.9 kcal mol^{-1} for RM systems with w_0 = 5 and 10 respectively.[42] The value obtained in the present study is thus similar to the RM systems with the same interlayer separation ($d = l$). Note that the E_{act} values are comparably smaller than the hydrogen bond energy for bulk water (7–9 kcal mol^{-1}). The E_{act} values obtained from these studies strongly depend upon the location of the probe. The probe used in the present study, C-500 provides information only from the AOT-water interface in both RM and lamellar systems. Thus it can experience all the transitions occurring at the interface involving IFW, IBW and bulk-type water. As reported earlier[42,64,65] the IBW and IFW hydrogen bond energy is smaller (in the range of 2.4-4 kcal mol^{-1}) compared to that in the bulk, and thus the E_{act} values obtained in the present study is smaller compared to that expected in the case of bulk water. We previously reported an E_{act} value of 7.4 kcal mol^{-1} with $w_0 = 10$ system using an water soluble probe, ANS, which provides information on the bulk water only. Also, note that the E_{act} value is higher for $L_0 = 46$ compared to $L_0 = 36$, and the difference is attributed to the higher fraction of bulk water present in the former systems. The similarity in the water structure at the AOT lamellar and RM system signifies the similarity in the water structure at the AOT interface of these two morphologically different systems which is also manifested in the identical <τ> values observed (Table 1).

Conclusion

We have explored the slow dynamics of water confined in AOT lamellar structures and RM with various degrees of hydration based on two criteria: similar surface to surface distance ($d = l$) and having the same number of water molecules per AOT molecule ($w_0 = L_0$) using picosecond-resolved fluorescence spectroscopy. It is observed that the relaxation dynamics of water of the lamellar systems is slower for the $w_0 = L_0$ systems but faster or comparable for the $d = l$ systems (Fig. 4). The differences in the timescale for these different systems can be understood as an optimization of several accelerating and retarding factors which involves the hydrogen bond strength (especially in the curved surface where the carbonyl carbon of AOT can participate in the bond formation), diffusion coefficient of water and the fraction of bulk water present in the systems. While the first two factors depend upon the morphology (geometry) of the surface, the latter one is dependent on the interlayer separation. The overall dynamics of relaxation of water is an optimization between these opposing factors. Our study strongly concludes the fact that both the morphology and the interlayer separation in these nanoconfining macromolecular systems play equally important roles in determining the dynamics of water relaxation.

Acknowledgements

P.K.V. thanks CSIR for fellowship. We thank DST for the financial support (SR/SO/BB-15/2007).

References

1 N. E. Levinger, *Curr. Opin. Colloid Interface Sci.*, 2000, **5**, 118–124.
2 K. Bhattacharyya, *Acc. Chem. Res.*, 2003, **36**, 95–101.
3 N. Sarkar, K. Das, A. Datta, S. Das and K. Bhattacharyya, *J. Phys. Chem.*, 1996, **100**, 10523–10527.
4 S. Sen, P. Dutta, D. Sukul and K. Bhattacharyya, *J. Phys. Chem. A*, 2002, **106**, 6017–6023.
5 P. Hazra, D. Chakrabarty, A. Chakraborty and N. Sarkar, *Chem. Phys. Lett.*, 2003, **382**, 71–80.
6 R. E. Riter, D. M. Willard and N. E. Levinger, *J. Phys. Chem. B*, 1998, **102**, 2705–2714.
7 D. Pant, R. E. Riter and N. E. Levinger, *J. Chem. Phys.*, 1998, **109**, 9995–10003.
8 D. E. Moilanen, N. E. Levinger, D. B. Spry and M. D. Fayer, *J. Am. Chem. Soc.*, 2007, **129**, 14311–14318.
9 I. R. Piletic, D. E. Moilanen, D. B. Spry, N. E. Levinger and M. D. Fayer, *J. Phys. Chem. A*, 2006, **110**, 4985–4999.

10 J. H. Fendler, E. J. Fendler, R. T. Medary and V. A. Woods, *J. Am. Chem. Soc.*, 1972, **94**, 7288–7295.
11 M. L. Stahla, B. Baruah, D. M. James, M. D. Johnson, N. E. Levinger and D. C. Crans, *Langmuir*, 2008, **24**, 6027–6035.
12 I. R. Piletic, D. E. Moilanen, N. E. Levinger and M. D. Fayer, *J. Am. Chem. Soc.*, 2006, **128**, 10366–10367.
13 M. Hu and L. Kevan, *J. Phys. Chem.*, 1990, **94**, 5348–5351.
14 M. Zulauf and H.-F. Eicke, *J. Phys. Chem.*, 1979, **83**, 480–486.
15 A. M. Howe, C. Toprakcioglu, J. C. Dore and B. H. Robinson, *J. Chem. Soc., Faraday Trans. 1*, 1986, **82**, 2411–2422.
16 N. Gorski and Y. M. Oatanevich, *Journal de Physique IV*, 1993, **03**, 149–152.
17 M. D. Angelo, D. Fioretto, G. Onori, L. Palmieri and A. Santucci, *Phys. Rev. E: Stat. Phys., Plasmas, Fluids, Relat. Interdiscip. Top.*, 1996, **54**, 993–996.
18 Y. Yoshimura, I. Abe, M. Ueda, K. Kajiwara, T. Hori and Z. A. Schelly, *Langmuir*, 2000, **16**, 3633–3635.
19 X. Shen, H. Gao and X. Wang, *Phys. Chem. Chem. Phys.*, 1999, **1**, 463–469.
20 J. Faeder and B. M. Ladanyi, *J. Phys. Chem. B*, 2005, **109**, 6732–6740.
21 E. M. Corbeil, R. E. Riter and N. E. Levinger, *J. Phys. Chem. B*, 2004, **108**, 10777–10784.
22 N. M. Correa and N. E. Levinger, *J. Phys. Chem. B*, 2006, **110**, 13050–13061.
23 R. Jimenez, G. R. Fleming, P. V. Kumar and M. Maroncelli, *Nature*, 1994, **369**, 471–473.
24 D. M. Willard, R. E. Riter and N. E. Levinger, *J. Am. Chem. Soc.*, 1998, **120**, 4151–4160.
25 D. M. Willard and N. E. Levinger, *J. Phys. Chem. B*, 2000, **104**, 11075–11080.
26 D. Pant and N. E. Levinger, *Langmuir*, 2000, **16**, 10123–10130.
27 D. E. Moilanen, E. E. Fenn, D. Wong and M. D. Fayer, *J. Chem. Phys.*, 2009, **131**, 014704–014709.
28 R. K. Mitra, S. S. Sinha, P. K. Verma and S. K. Pal, *J. Phys. Chem. B*, 2008, **112**, 12946–12953.
29 C. Boissière, J. B. Brubach, A. Mermet, G. de Marzi, C. Bourgaux, E. Prouzet and P. Roy, *J. Phys. Chem. B*, 2002, **106**, 1032–1035.
30 K. Fontell, *J. Colloid Interface Sci.*, 1973, **44**, 318–319.
31 N. Casillas, J. E. Puig, R. Olayo, T. J. Hart and E. I. Frames, *Langmuir*, 1989, **5**, 384–389.
32 I. Åslund, C. Cabaleiro-Lago, O. Soderman and D. Topgaard, *J. Phys. Chem. B*, 2008, **112**, 2782–2794.
33 P. L. Hubbard, K. M. McGrath and C. P. T., *J. Phys. Chem. B*, 2006, **110**, 20781–20788.
34 P. T. Callaghan and O. Soderman, *J. Phys. Chem.*, 1983, **87**, 1737–1744.
35 R. Angelico, B. Balinov, A. Ceglie, U. Olsson, G. Palazzo and O. Soderman, *Langmuir*, 1999, **15**, 1679–1684.
36 L. J. Schwartz, C. L. DeCiantis, S. Chapman, B. K. Kelley and J. P. Hornak, *Langmuir*, 1999, **15**, 5461–5466.
37 I. D. Charlton and A. P. Doherty, *J. Phys. Chem. B*, 2000, **104**, 8061–8067.
38 D. E. Moilanen, E. E. Fenn, D. Wong and M. D. Fayer, *J. Am. Chem. Soc.*, 2009, **131**, 8318–8328.
39 L. Coppola, R. Muzzalupo, G. A. Ranieri and M. Terenzi, *Langmuir*, 1995, **11**, 1116–1121.
40 N. Nandi and B. Bagchi, *J. Phys. Chem. B*, 1997, **101**, 10954–10961.
41 S. Sen, S. Mukherjee, A. Halder and K. Bhattacharyya, *Chem. Phys. Lett.*, 2004, **385**, 357–361.
42 P. K. Verma, A. Makhal, R. K. Mitra and S. K. Pal, *Phys. Chem. Chem. Phys.*, 2009, **11**, 8467–8476.
43 J. R. Lakowicz, *Principles of fluorescence spectroscopy*, Kluwer Academic/Plenum, New York, 1999.
44 M. L. Horng, J. A. Gardecki, A. Papazyan and M. Maroncelli, *J. Phys. Chem.*, 1995, **99**, 17311–17337.
45 D. V. O'Conner and D. Philips, *Time Correlated Single Photon Counting*, Academic Press, London, 1984.
46 S. K. Pal, J. Peon, B. Bagchi and A. H. Zewail, *J. Phys. Chem. B*, 2002, **106**, 12376–12395.
47 P. Majumder, R. Sarkar, A. K. Shaw, A. Chakraborty and S. K. Pal, *J. Colloid Interface Sci.*, 2005, **290**, 462–474.
48 D. Banerjee, P. K. Verma and S. K. Pal, *Photochem. Photobiol. Sci.*, 2009, **8**, 1441–1447.
49 R. K. Mitra, S. S. Sinha and S. K. Pal, *Langmuir*, 2008, **24**, 49–56.
50 M. Wong, J. K. Thomas and T. Nowak, *J. Am. Chem. Soc.*, 1977, **99**, 4730–4736.
51 M. Wong, J. K. Thomas and M. Graetzel, *J. Am. Chem. Soc.*, 1976, **98**, 2391–2397.
52 H. Hauser, G. Haering, A. Pande and P. L. Luisi, *J. Phys. Chem.*, 1989, **93**, 7869–7876.
53 H.-F. Eicke and J. Rehak, *Helv. Chim. Acta*, 1976, **59**, 2883–2891.
54 P. K. Verma, R. M. Mitra and S. K. Pal, *Langmuir*, 2009, **25**, 11336–11343.
55 D. Cringus, A. Bakulin, J. Lindner, P. Voehringer, M. S. Pshenichnikov and D. A. Wiersma, *J. Phys. Chem. B*, 2007, **111**, 14193–14207.
56 D. Cringus, J. Lindner, M. T. W. Milder, M. S. Pshenichnikov, P. Vöhringer and D. A. Wiersma, *Chem. Phys. Lett.*, 2005, **408**, 162–168.
57 D. S. Venables, K. Huang and C. A. Schmuttenmaer, *J. Phys. Chem. B*, 2001, **105**, 9132–9138.
58 J. Faeder and B. M. Ladanyi, *J. Phys. Chem. B*, 2000, **104**, 1033–1046.
59 I. R. Piletic, H.-S. Tan and M. D. Fayer, *J. Phys. Chem. B*, 2005, **109**, 21273–21284.
60 N. Nandi, K. Bhattacharyya and B. Bagchi, *Chem. Rev.*, 2000, **100**, 2013–2045.
61 K. B. Bhattacharyya and B., *J. Phys. Chem. A*, 2000, **104**, 10603–10613.
62 N. Nandi and B. Bagchi, *J. Phys. Chem. A*, 1998, **102**, 8217–8221.
63 R. Biswas and B. Bagchi, *J. Phys. Chem. A*, 1999, **103**, 2495–2500.
64 R. K. Mitra, S. S. Sinha and S. K. Pal, *J. Phys. Chem. B*, 2007, **111**, 7577–7581.
65 S. Pal, S. Balasubramanian and B. Bagchi, *J. Phys. Chem. B*, 2003, **107**, 5194–5202.